TWO-PHOTON CROSS-SECTIONS FROM THE SATURATION MODEL*

J. Kwieciński[a], L. Motyka[b,c] and N. Tîmneanu[b]

[a]Henryk Niewodniczański Institute of Nuclear Physics
Radzikowskiego 152, 31-342 Kraków, Poland
[b]High Energy Physics, Uppsala University, Uppsala, Sweden
[c]Marian Smoluchowski Institute of Physics, Jagellonian University
Reymonta 4, 30-059 Kraków, Poland

(Received April 11, 2002)

A saturation model for the total $\gamma\gamma$ and $\gamma^*\gamma^*$ cross-sections and for the real photon structure function $F_2^\gamma(x,Q^2)$ is described. The model is based on a QCD dipole picture of high energy scattering. The two-dipole cross-section is assumed to satisfy the saturation property with the saturation radius taken from the GBW analysis of the γ^*p interaction at HERA. The model is combined with the QPM and non-pomeron reggeon contributions and it gives a very good description of the data on the $\gamma\gamma$ total cross-section, on the photon structure function $F_2^\gamma(x,Q^2)$ at low x and on the $\gamma^*\gamma^*$ cross-section. Production of heavy quarks in $\gamma\gamma$ collisions is also studied.

PACS numbers: 12.90.+b

1. Introduction

The saturation model [1] was proven to provide a very efficient framework to describe variety of experimental results on high energy scattering. With a very small number of free parameters, Golec-Biernat and Wüsthoff (GBW) fitted low x data from HERA for both inclusive and diffractive scattering [1]. Some promising results were also obtained for elastic vector meson photo- and electroproduction [2].

The central concept behind the saturation model is an x dependent saturation scale $Q_s(x)$ at which unitarity corrections to the linear parton evolution in the proton become significant. In other words, $Q_s(x)$ is a typical scale of a hard probe at which a transition from a single scattering to a multiple scattering regime occurs.

* Presented by L. Motyka at the Cracow Epiphany Conference on Quarks and Gluons in Extreme Conditions, Cracow, Poland, January 3–6, 2002.

The model is well grounded in perturbative QCD. The existence of such a scale in the saturation domain was suggested already in [3] as a consequence of the GLR equation [4] obtained in the double logarithmic approximation. A parton evolution equation involving unitarity corrections at LL-$1/x$ approximation and the large-N_c limit was derived by Balitsky and Kovchegov (BK) [5]. Numerous studies [6] showed that the solutions to the BK equation are, with a good approximation, consistent with the presence of the saturation scale.

Our idea was to extend the saturation model constructed for $\gamma^* p$ scattering to describe also $\gamma^*\gamma^*$ cross sections. The successful extension, performed in [7], provided a test of the saturation model in a new environment and confirmed the universality of the model. Results obtained in [7] are also of some importance for two-photon physics, since the model is capable of describing a broad set of observables in wide kinematical range in a simple, unified framework. In this presentation the most important results of [7] will be summarized.

2. The model

The saturation model for two-photon interactions is constructed in analogy to the GBW model [1]. In terms of the virtual photon four-momenta q_1 and q_2 we have $Q^2_{1,2} = -q^2_{1,2}$ and $W^2 = (q_1 + q_2)^2$, see Fig. 1. Each of the virtual photons is decomposed into colour dipoles $(q\bar{q})_{\rm dipole}$ representing virtual components of the photon in the transverse plane and their distribution in the photon is assumed to follow from the perturbative formalism.

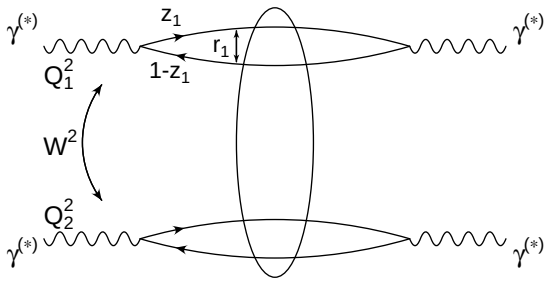

Fig. 1. The diagram illustrating the $\gamma^*\gamma^*$ interaction in the dipole representation.

A formula for the two-photon cross-section part coming from the exchange of *gluonic* degrees of freedom reads [8]

$$\sigma^G_{ij}(W^2, Q^2_1, Q^2_2) =$$

$$\sum_{a,b=1}^{N_f} \int_0^1 dz_1 \int d^2\boldsymbol{r}_1 \left|\Psi^a_i(z_1, \boldsymbol{r}_1)\right|^2 \int_0^1 dz_2 \int d^2\boldsymbol{r}_2 \left|\Psi^b_j(z_2, \boldsymbol{r}_2)\right|^2 \sigma^{dd}_{a,b}(\bar{x}_{ab}, r_1, r_2)\,, \quad (1)$$

where the indices i, j label the polarisation states of the virtual photons, *i.e.* T or L and $\sigma^{dd}_{a,b}(\bar{x}_{ab}, r_1, r_2)$ are the dipole–dipole total cross-sections corresponding to their different flavour content specified by a and b. The transverse vectors $\boldsymbol{r}_k$ denote the separation between q and $\bar{q}$ in the colour dipoles and z_k are the longitudinal momentum fractions of the quark in the photon k ($k = 1, 2$). The photon wave functions are given by

$$\begin{aligned} \left|\Psi^a_T(z, \boldsymbol{r})\right|^2 &= \frac{6\alpha_{em}}{4\pi^2}\, e_a^2 \left\{ \left[z^2 + (1-z)^2\right] \varepsilon_a^2 K_1^2(\varepsilon_a r) + m_f^2\, K_0^2(\varepsilon_a r) \right\}, \\ \left|\Psi^a_L(z, \boldsymbol{r})\right|^2 &= \frac{6\alpha_{em}}{\pi^2}\, e_a^2 Q^2 z^2 (1-z)^2 K_0^2(\varepsilon_a r), \end{aligned} \tag{2}$$

with

$$\left(\varepsilon^k_a\right)^2 = z_k\,(1-z_k)\,Q^2 + m_a^2, \qquad k = 1, 2, \tag{3}$$

where e_a and m_a denote the charge and mass of the quark of flavour a. The functions K_0 and K_1 are the McDonald–Bessel functions.

Inspired by the GBW simple choice for the dipole–proton cross-section, we use the following parametrisation of the dipole–dipole cross-section $\sigma_{a,b}$

$$\sigma^{dd}_{a,b}(\bar{x}_{ab}, r_1, r_2) = \sigma_0^{a,b} \left[1 - \exp\left(-\frac{r^2_{\text{eff}}}{4R_0^2(\bar{x}_{ab})}\right)\right], \tag{4}$$

where for $\bar{x}_{ab}$ we take the following expression symmetric in (1), (2)

$$\bar{x}_{ab} = \frac{Q_1^2 + Q_2^2 + 4m_a^2 + 4m_b^2}{W^2 + Q_1^2 + Q_2^2}, \tag{5}$$

which allows an extension of the model down to the limit $Q^2_{1,2} = 0$. Note, that $\bar{x}_{ab}$ depends on the flavour of scattering quarks. We use the same parametrisation of the saturation radius $R_0(\bar{x})$ as that in Eq. (7) in [1], *i.e.*

$$R_0(\bar{x}) = \frac{1}{Q_0}\left(\frac{\bar{x}}{x_0}\right)^{\lambda/2} \tag{6}$$

and adopt the same set of parameters defining this quantity as those in [1]. For the saturation value $\sigma_0^{a,b}$ of the dipole–dipole cross-section (*cf.* Eq. (4)) we set

$$\sigma_0^{a,b} = \frac{2}{3}\sigma_0, \tag{7}$$

where σ_0 is the same as that in [1]. For light flavours, Eq. (7) can be justified by the quark counting rule, as the ratio between the number of constituent quarks in a photon and the corresponding number of constituent quarks in the proton. We also use the same value of $\sigma_0^{a,b}$ for all flavours.

Three scenarios for $r_{\rm eff}(r_1, r_2)$ are considered:

(1) $r^2_{\rm eff} = \frac{r_1^2 r_2^2}{r_1^2 + r_2^2}$,

(2) $r^2_{\rm eff} = \min\left(r_1^2, r_2^2\right)$,

(3) $r^2_{\rm eff} = \min\left(r_1^2, r_2^2\right)\left[1 + \ln\left(\frac{\max(r_1,r_2)}{\min(r_1,r_2)}\right)\right]$.

All three parametrisations exhibit colour transparency, *i.e.* $\sigma^{dd}_{a,b}(\bar{x}, r_1, r_2) \to 0$ for $r_1 \to 0$ or $r_2 \to 0$. Cases (1) and (2) reduce to the original GBW model when one of the dipoles is much larger than the other and option (3), being significantly different from (1) and (2), is a control case.

The saturation model accounts for an exchange of *gluonic* degrees of freedom, the QCD pomeron fan diagrams. Such exchanges dominate at very high energies (low x) but at lower energies the processes involving quark exchange have to be considered as well. Thus, in order to get a complete description of $\gamma^*\gamma^*$ interactions we should add to the "pomeron" contribution defined by Eq. (1) the non-pomeron reggeon and QPM terms [9]. The additional contributions are characterised by a decreasing energy dependence, *i.e.* $\sim 1/W^{2\eta}$ for the reggeon and $\sim 1/W^2$ (with $\ln W$ corrections) for QPM. The QPM contribution, represented by the quark box diagrams, is well known and the cross-sections are given, for instance, in [10]. The reggeon contribution represents a non-perturbative phenomenon related to Regge trajectories of light mesons. It is known mainly from fits to total hadronic cross-sections and to the proton structure function F_2. We used the following parametrisation of the reggeon exchange cross-section in two-photon interactions [8]

$$\sigma^R(W^2, Q_1^2, Q_2^2) = 4\pi^2 \alpha_{em}^2 \frac{A_2}{a_2}\left[\frac{a_2^2}{(a_2 + Q_1^2)(a_2 + Q_2^2)}\right]^{1-\eta}\left(\frac{W^2}{a_2}\right)^{-\eta}. \quad (8)$$

We have chosen $\eta = 0.3$ in accordance with the value of the Regge intercept of the f_2 meson trajectory $1 - \eta = 0.7$ [11]. Parameters A_2 and a_2 were fitted to the data on two-photon collisions.

Formulae (1) and (8) describing the gluonic and reggeon components are valid at asymptotically high energies, where the impact of kinemetical thresholds is small. The threshold effects are approximately accounted for by introducing a multiplicative correction factors, whose form is deduced from spectator counting rules (see [7]).

Thus, the total $\gamma^*(Q_1^2)\gamma^*(Q_2^2)$ cross-section reads

$$\sigma_{ij}^{\rm tot} = \tilde{\sigma}_{ij}^{G} + \tilde{\sigma}^{R}\delta_{iT}\delta_{jT} + \sigma_{ij}^{\rm QPM}\,, \tag{9}$$

where $\tilde{\sigma}_{ij}^{G}(W^2, Q_1^2, Q_2^2)$ is the gluonic component, corresponding to dipole–dipole scattering, as in Eq. (1), but with the dipole–dipole cross-section including the threshold correction factor

$$\tilde{\sigma}_{a,b}^{dd}\left(\bar{x}_{ab}, r_1, r_2\right) = \left(1-\bar{x}_{ab}\right)^5\ \sigma_{a,b}^{dd}\left(\bar{x}_{ab}, r_1, r_2\right)\,, \tag{10}$$

cf. Eq. (4), and $\bar{x}_{ab}$ is given by Eq. (5). The sub-leading reggeon contributes only to scattering of two transversely polarised photons and also contains a threshold correction

$$\tilde{\sigma}^{R}(W^2, Q_1^2, Q_2^2) = (1-\bar{x})\,\sigma^{R}(W^2, Q_1^2, Q_2^2)\,, \tag{11}$$

with

$$\bar{x} = \frac{Q_1^2 + Q_2^2 + 8m_q^2}{W^2 + Q_1^2 + Q_2^2}\,. \tag{12}$$

The third term $\sigma_{i,j}^{\rm QPM}(W^2, Q_1^2, Q_2^2)$ is the standard QPM contribution.

3. Comparison to experimental data

3.1. Parameters of models

In the comparison to the data we study three models, based on all cases for the effective radius, as described in Section 2.2. We will refer to these models as Model 1, 2 and 3, corresponding to the choice of the dipole–dipole cross-section. Let us recall that we take without any modification the parameters of the GBW model: $\sigma_0 = 29.13$ mb, $x_0 = 0.41 \times 10^{-4}$ and $\lambda = 0.277$. However, we fit the light quark mass to the two-photon data, since it is not very well constrained by the GBW fit, as we explicitly verified. On the other hand, the sensitivity of the choice of the mass appears to be large for the two-photon total cross-section. We find that the optimal values of the light quark (u, d and s) masses m_q are 0.21, 0.23 and 0.30 GeV in Model 1, 2 and 3 correspondingly. Also, the masses of the charm and bottom quark are tuned within the range allowed by current measurements, to get the optimal global description in Model 1, $r_{\rm eff}^2 = r_1^2 r_2^2/(r_1^2 + r_2^2)$, which agrees best with the data. For the charm quark we use $m_c = 1.3$ GeV and for bottom $m_b = 4.5$ GeV. The values of parameters in the reggeon term (8): $\eta = 0.3$, $A_2 = 0.26$ and $a_2 = 0.2$ GeV^2 are found to give the best description of data, when combined with the saturation model. The

values of masses listed above are consistently used also in the quark box contribution (QPM). The Models, which we shall mention from now on, contain the saturation models described in Section 2, combined with the reggeon and QPM contribution.

The references to the relevant experimental papers may be found in [7].

3.2. The test case: the γp total cross-section

In order to describe two-photon data, we altered the original light quark mass of the GBW model. Besides that, we included the reggeon term and the threshold correction factors in the analysis. Thus, it is worth-while to compare the results from the modified model with the data on the γp total cross-section. Thus we calculated the dipole–proton scattering contribution using the original GBW approach, with the light quark mass, m_q, set to 0.21 GeV, as in Model 1, and added the reggeon term

$$\sigma_{\gamma p}^{R}(W^2) = A_{\gamma p} \left(\frac{W^2}{1\,\mathrm{GeV}^2} \right)^{-\eta}, \tag{13}$$

where $A_{\gamma p}$ was fitted to the data and the best value reads $A_{\gamma p} = 0.135$ mb. The result is given in Fig. 2, where the cross-section from Model 1 is compared to the experimental data and to the classical Donnachie–Landshoff fit [12]. The fitted curve, with only one free parameter $A_{\gamma p}$ follows the data accurately, suggesting that the model has certain universal properties.

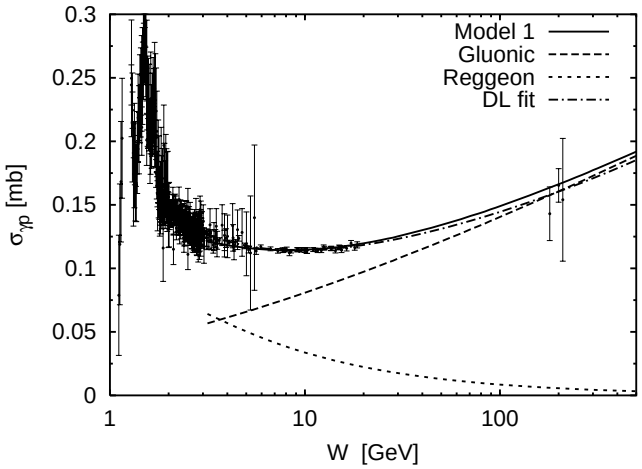

Fig. 2. The total γp cross-section — predictions from the GBW model with the light quark mass m_q set to 0.21 GeV and the charmed quark mass $m_c = 1.3$ GeV, supplemented by the reggeon term (13), compared to the data and to the Donnachie–Landshoff fit.

3.3. Total $\gamma\gamma$ cross-section

The available data for the $\gamma\gamma$ total cross-section range from the $\gamma\gamma$ energy W being equal to about 1 GeV up to about 160 GeV, see Fig. 3. The experimental errors of the data are, unfortunately, rather large. One of the reasons is that those data were taken for virtual photons coming from electron beams and then the results were extrapolated to zero virtualities. Some uncertainty is caused by the reconstruction of actual $\gamma\gamma$ collision energy from the visible hadronic energy. In such a reconstruction one relies on an unfolding procedure, based on a Monte Carlo programme. In Fig. 3 we show the total $\gamma\gamma$ cross-section from the Models, obtained using Eq. (9) with $i = j = T$. The data from LEP were unfolded with PHOJET. The agreement with the data is very good down to $W \simeq 3$ GeV for all the Models.

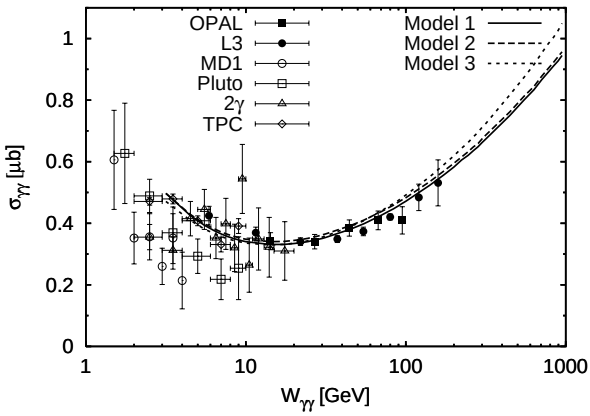

Fig. 3. The total $\gamma\gamma$ cross-section: data compared with predictions from all three Models.

3.4. Total $\gamma^*\gamma^*$ cross-section

The data for the total $\gamma^*\gamma^*$ cross-section are extracted from so-called double-tagged events, that is from e^+e^- events in which both the scattered electrons are measured and hadrons are produced. In such events measurement of the kinematical variables of the leptons determines both the virtualities Q_1^2 and Q_2^2 of the colliding photons and the collision energy W. The tagging angles in LEP experiments restrict the virtualities to be similar, *i.e.* $Q_1^2 \sim Q_2^2 = Q^2$. The data are available from LEP for average values $Q^2 = 3.5$ GeV^2, 14 GeV^2 and $Q^2 = 17.9$ GeV^2 in a wide range of W.

In Figs. 4 (a), (b), (c) those data are compared with the curves from the Models. As an estimate of the total $\gamma^*\gamma^*$ cross-section we use a simple sum of the cross-sections $\sigma_{ij}^{\rm tot}$ (Eq. (9)) over transverse and longitudinal

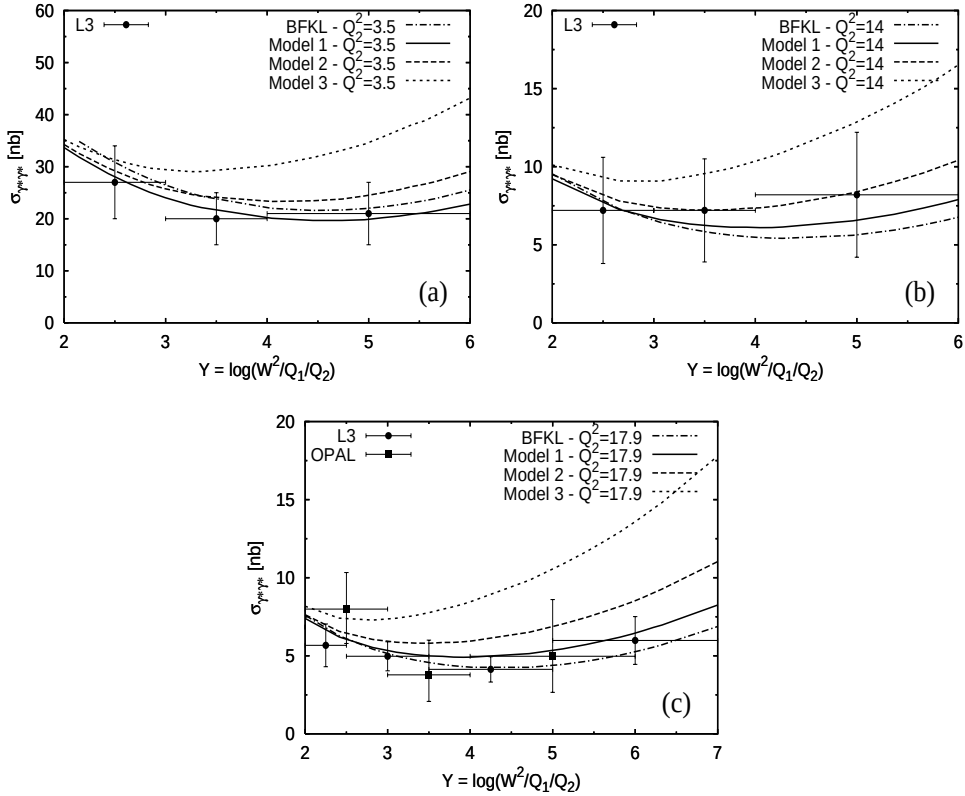

Fig. 4. Total $\gamma^*\gamma^*$ cross-section for (a) $Q^2 = 3.5$ GeV^2, (b) $Q^2 = 14$ GeV^2 and (c) $Q^2 = 17.9$ GeV^2 — comparison between LEP data and the Models plotted as a function of $Y = \ln(W^2/Q^2)$. Also shown is the result of Ref. [9] based on the BFKL formalism with sub-leading corrections, supplemented by the QPM term, the soft pomeron and the sub-leading reggeon contributions.

polarisations i and j of both photons. In addition we plot also the prediction obtained in Ref. [9] by solving the BFKL equation with non-leading effects, and added phenomenological soft pomeron and reggeon contributions and the QPM term. Models 1 and 2 fit the data well whereas Model 3 does not.

The virtuality of both photons are large, so the unitarity corrections, the light quark mass effects and the reggeon contribution are not important here. Moreover, the perturbative approximation for the photon wave function is fully justified in this case. Thus, in this measurement the form of the dipole–dipole cross-section is directly probed.

3.5. Photon structure

The data on quasi-real photon structure are obtained mostly in single tagged e^+e^- events, in which a two-photon collision occurs. One of the photons has a large virtuality and probes the other, almost real photon.

In Fig. 5 we show the comparison of our predictions with the experimental data for the virtuality Q^2 in the range from (a) 1.9 to 2.8 GeV^2, (b) 3.7 to 5.1 GeV^2, (c) 8.9 to 12.0 GeV^2 and finally, (d) from 16.0 to 23.1 GeV^2. Note, that in each plot the data for various virtualities are combined. In each plot the value of virtuality Q^2 adopted to obtain the theoretical curve is indicated and was selected to match the average value Q^2 of the data-set containing the best data at low x. Model 1, favoured by the $\gamma^*\gamma^*$ data provides the best description of F_2^γ as well.

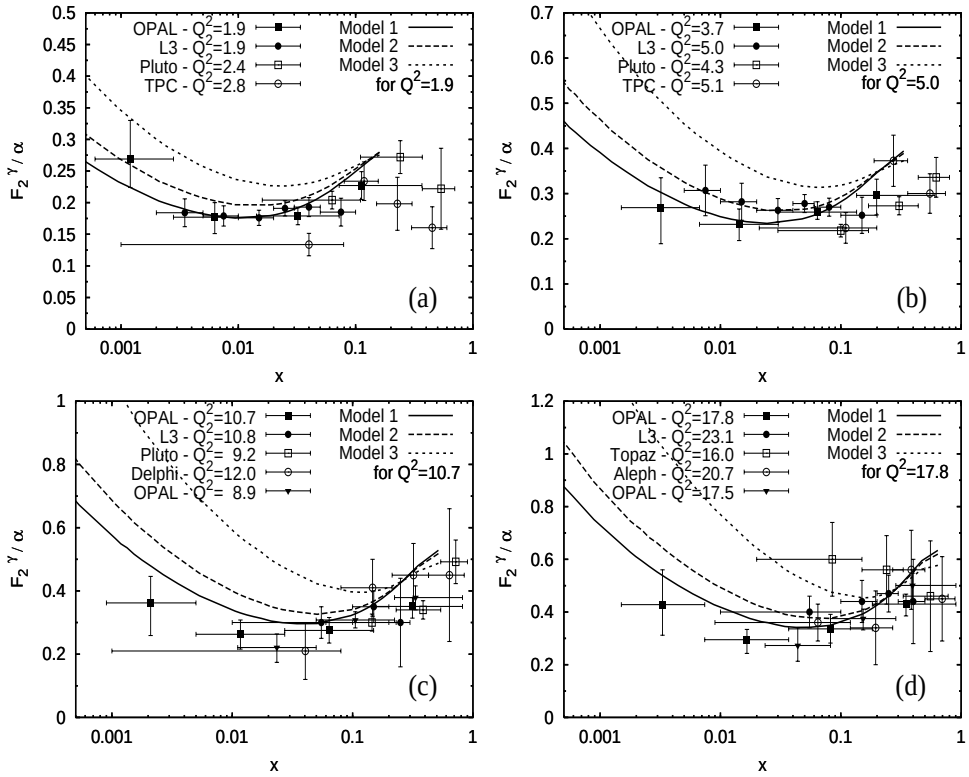

Fig. 5. The photon structure function $F_2^\gamma(x, Q^2)$: the experimental data compared to predictions following from the Models for various Q^2: (a) from 1.9 to 2.8 GeV^2, (b) from 3.7 to 5.1 GeV^2, (c) from 8.9 to 12.0 GeV^2 and (d) from 16.0 to 23.1 GeV^2.

3.6. Heavy flavour production

Another interesting process which we have studied in the dipole model is the production of heavy flavours (charm and bottom) in $\gamma\gamma$ collisions. Heavy quarks can be produced by three mechanisms: a direct production, a direct photoproduction off a resolved photon and a process with two resolved photons. The last mechanism is not accounted for in our approach.

The reggeon exchange is a non-perturbative phenomenon and should not contribute to heavy flavour production, so it is assumed to vanish here. In Fig. 6 we plot the predictions from all three Models compared with L3 data on charm production. The best model, Model 1, is slightly below the data. The shape of the cross-section is well reproduced.

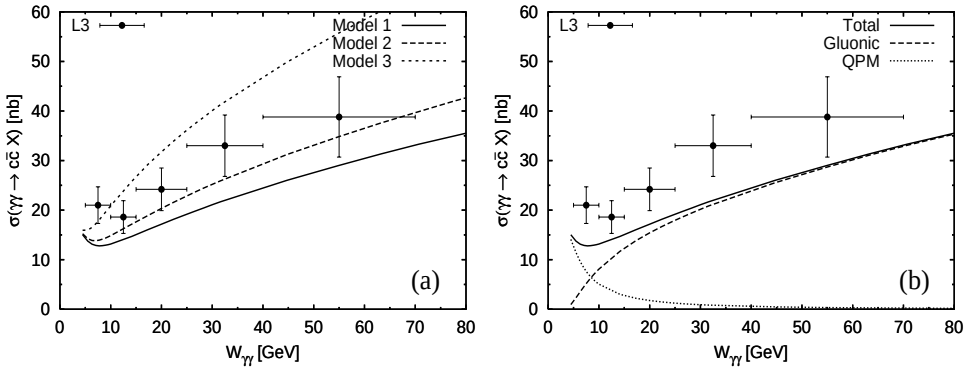

Fig. 6. The cross section for the inclusive charm production in $\gamma\gamma$ collisions: (a) results for all three Models and (b) the decomposition of the result from Model 1 on the QPM and gluonic component.

Production of bottom quarks in two almost real photon collisions was investigated experimentally by the L3 and the OPAL collaborations. There, the measured process was $e^+e^- \to e^+e^- b\bar{b}X$, with anti-tagged electrons at e^+e^- invariant collision energies $\sqrt{s}_{ee}$ between 189 GeV and 202 GeV. The total cross-section for this reaction was found to be $13.1 \pm 2.0\,(\text{stat}) \pm 2.4\,(\text{syst})\,\text{pb}$ (L3) and $14.2 \pm 2.5\,(\text{stat}) \pm 5\,(\text{syst})\,\text{pb}$ (OPAL) whereas the theoretical estimate from Model 1 for $\sqrt{s}_{ee} = 200$ GeV gives about 5.5 pb with less than 10% uncertainty related to the choice of b-quark mass. This is significantly below the experimental data but above the expectations of $3 \pm 1\,\text{pb}$ based on standard QCD calculations with the use of the resolved photon approximation.

In conclusion, the saturation model underestimates the cross-section for production of heavy quarks and the discrepancy increases with increasing quark mass, or perhaps, decreasing electric charge.

4. Conclusions

In this contribution an extension of the saturation approach to two-photon physics has been presented. This extension required an explicit model for the scattering of two colour dipoles. We considered three models of this cross-section, all of them exhibiting the essential feature of colour transparency for small dipoles, and the saturation property for large ones. We kept the GBW form of the unitarising function and the original parameters, except for changing the values of quark masses, which was necessary to describe the data on the total two real photon cross-section. In order to obtain a more complete description applicable at lower energies the saturation model has been combined with other, well known contributions related to the quark box diagram and non-pomeron reggeon exchange.

Our theoretical results were compared with the data for different two-photon processes at high rapidity values: the total $\gamma\gamma$ cross-section, the total $\gamma^*\gamma^*$ cross-section for similar virtualities of the photons, the real photon structure function F_2^γ and heavy flavour production. Free parameters were fitted to the data. With the best model a reasonable global description of the available two-photon data was obtained, except for the b-quark production. Thus, the saturation model was found to provide a simple and efficient framework to calculate observables in two-photon processes.

We gratefully acknowledge the support from the Swedish Natural Science Research Council and by the Polish State Committee for Scientific Research (KBN) grants no. 2P03B 05119 and 5P03B 14420.

REFERENCES

[1] K. Golec-Biernat, M. Wüsthoff, *Phys. Rev.* **D59**, 014017 (1998); *Phys. Rev.* **D60**, 114023 (1999).

[2] A.C. Caldwell, M.S. Soares, *Nucl. Phys.* **A696**, 125 (2001).

[3] J. Bartels, E.M. Levin, *Nucl. Phys.* **B387**, 617 (1992).

[4] L.V. Gribov, E.M. Levin, M.G. Ryskin, *Phys. Rep.* **100**, 1 (1983).

[5] Ia. Balitsky, *Nucl. Phys.* **B463**, 99 (1996); Yu. V. Kovchegov, *Phys. Rev.* **D60**, 034008 (1999).

[6] See *e.g.* Yu.V. Kovchegov, *Phys. Rev.* **D61**, 074018 (2000); E. Levin, K. Tuchin, *Nucl. Phys.* **B573**, 833 (2000); N. Armesto, M.A. Braun, *Eur. Phys. J.* **C20**, 517 (2001); K. Golec-Biernat, L. Motyka, A.M. Staśto, *Phys. Rev.* **D65**, 074037 (2002).

[7] N. Tîmneanu, J. Kwieciński, L. Motyka, `hep-ph/0110409`.

[8] A. Donnachie, H.G. Dosch, M. Rueter, *Eur. Phys. J.* **C13**, 141 (2000).

[9] J. Kwieciński, L. Motyka, *Acta Phys. Pol.* **B30**, 1817 (1999); *Phys. Lett.* **B462**, 203 (1999); *Eur. Phys. J.* **C18**, 343 (2000).

[10] V.M. Budnev, I.F. Ginzburg, C.V. Meledin, V.G. Serbo, *Phys. Rep.* **15**, 181 (1974).

[11] P.V. Landshoff, `hep-ph/0010315`.

[12] A. Donnachie, P.V. Landshoff, *Phys. Lett.* **B296**, 227 (1992); *Z. Phys.* **C61**, 139 (1994).